www.sciencemag.org/cgi/content/full/science.1223532/DC1

# Supplementary Materials for

## Long-Range Incommensurate Charge Fluctuations in (Y,Nd)$Ba_2Cu_3O_{6+x}$

G. Ghiringhelli,* M. Le Tacon, M. Minola, S. Blanco-Canosa, C. Mazzoli, N. B. Brookes, G. M. De Luca, A. Frano, D. G. Hawthorn, F. He, T. Loew, M. Moretti Sala, D. C. Peets, M. Salluzzo, E. Schierle, R. Sutarto, G. A. Sawatzky, E. Weschke, B. Keimer,* L. Braicovich

*To whom correspondence should be addressed. E-mail: giacomo.ghiringhelli@fisi.polimi.it (G.G.); b.keimer@fkf.mpg.de (B.K.)

Published 12 July 2012 on *Science* Express
DOI: 10.1126/science.1223532

**This PDF file includes:**

## Materials and Methods

**Sample Preparation and Characterization** We used untwinned $YBa_2Cu_3O_{6.35}$, $YBa_2Cu_3O_{6.45}$, $YBa_2Cu_3O_{6.5}$, $YBa_2Cu_3O_{6.6}$, $YBa_2Cu_3O_7$ and $Y_{0.85}Ca_{0.15}Ba_2Cu_3O_7$ single crystals of volume about $3 \times 3 \times 0.5$ mm$^3$. The corresponding superconducting transition temperatures $T_c$ were determined for each crystal by SQUID magnetometry (see details in Methods section of Ref. (*40*)) and are listed in table S1.

The $YBa_2Cu_4O_8$ single crystals were obtained using KOH flux under ambient pressure in a box furnace. The source material was conventionally prepared polycrystalline $YBa_2Cu_3O_7$ mixed with CuO in a molar ratio of 1:1. The details are described in Refs. (*41, 42*). The crystal size was $0.8 \times 0.8 \times 0.2$ mm$^3$, and $T_c = 80$ K. Single crystals were polished in air to obtain a flat and shiny (001) surface.

$Nd_{1.2}Ba_{1.8}CuO_7$ films of thickness 50 nm and 100 nm and $NdBa_2CuO_7$ and $YBa_2CuO_7$ films of thickness 100 nm were deposited on $SrTiO_3$ (100) single crystals by diode high-pressure oxygen sputtering. In the former two cases the underdoping is determined by the 1.2/1.8 ratio in the Nd to Ba relative contents. The two doping levels and $T_c$ are a consequence of the different film thickness, as explained in Ref. (*43*). The optimally doped films were thick enough to neglect the influence of the substrate, which forces the thinner films to grow pseudo-tetragonally. The films had an area of approximatively 5 $\times$ 5 mm$^2$. Details of the films growth and characterization can be found in Ref. (*43*). The superconducting transition temperature was determined by DC four-point transport and by magnetic susceptibility measurements.

The oxygen content and the hole concentration $p$ were determined from the known doping dependence of the out-of-plane lattice parameter $c$ and of $T_c$ (*7*). For all samples, XAS and RXS measurements were performed without any in-vacuum surface preparation.

**Measurements** The energy resolved RXS measurements (RIXS) were performed at the ADRESS beam line (*44*) of the Swiss Light Source (Paul Scherrer Institute, Switzerland) using the *SAXES* spectrometer (*45*); and at the ID08 beamline of the European Synchrotron Radiation Facility (ESRF, Grenoble, France) using the *AXES* spectrometer (*46, 47*). The XAS measurements were made at the ID08 beamline of the ESRF, using the fast scanning *Dragon* monochromator. The energy integrated RXS measurements were performed at the UE46-PGM1 beam line of the Bessy-II storage ring (Helmholtz-Zentrum Berlin, Germany) using the XUV diffractometer.

The resonant conditions were achieved by tuning the energy of the incident x-ray to the maximum of the Cu $L_3$ absorption peak, around 931.5 eV. At that energy the absorption takes place mainly at the Cu2 sites with $3d^9$ electronic configuration. Although a contribution from Cu1 sites is also present around the same photon energy as demonstrated in Ref. (*24*), we can neglect it because its polarization dependence in the RXS process is expected to be different from that found in our data (Fig. 2A). The scattering geometry is shown in Fig. 1 B,C. While keeping the scattering angle ($2\theta$) fixed, the sample is turned around the $y$ axis, perpendicular to the scattering plane, thus changing the projection of the transferred momentum $\mathbf{q} = \mathbf{k} - \mathbf{k}'$ onto the direction $x$ parallel to the $CuO_2$ plane. This projection is the meaningful quantity $q_{//}$ for

the two-dimensional electron system of the layered cuprates. At 931.5 eV photon energy the total momentum transfer is $q = 0.944 \sin\theta$ Å$^{-1}$. In the RIXS experiments $2\theta = 130°$, giving $q = 0.855$ Å$^{-1}$, which allows one to cover about $\sim 85\%$ of the first Brillouin zone along the [100] direction (see Fig. 1C).

Momentum transfers are given in reciprocal lattice units (r.l.u.), that is, in units of the reciprocal lattice vectors $a^*$, $b^*$ and $c^*$ where $a^*$=2$\pi/a$, $b^*$=2$\pi/b$, and $c^*$=2$\pi/c$. (See table 1 for the values of $a$, $b$, and $c$ for each sample). The conventional sign of $q_{//}$ is shown in Fig. 1C: $q_{//} < 0$ ($q_{//} > 0$) for grazing incidence onto (emission from) the (001) surface. The total instrumental energy resolution was about 130 meV, experimentally determined on a non-resonant elastic scattering spectrum of polycrystalline graphite. The momentum resolution was $\sim 0.005$ r.l.u. Each spectrum was measured for 5 minutes. The (quasi)elastic intensity was determined by fitting the zero-energy-loss feature with a Gaussian peak of width not exceeding 1.3 times the instrumental energy width, to take into account possible fluctuations of the energy resolution and uncertainties related count statistics. That intensity was normalized to the integral of the RIXS spectrum between 0 and 20 eV energy loss (Fig. 1 D). In Fig. S2 we have plotted the raw RIXS intensity for the $YBa_2CuO_{6.6}$ sample at $T \simeq T_c$ = 61 K, where the signal is maximal, for three different momentum transfers: $q_{//}$=0.31 r.l.u. (on the superstructure peak) and $q_{//}$=0.28 r.l.u. and 0.35 r.l.u. (away from it). The differences between the former and each of the latter spectra are displayed in Figs. S2 B and C. Despite the limited energy resolution, we can safely place an upper bound of 20 meV for the energy of the CDW contribution to the elastic peak.

In the energy integrating experiments $2\theta = 154°$, $q$=0.919 Å$^{-1}$, $q_{//,\mathrm{max}}$=0.44 r.l.u. The scattered intensity was measured with a photodiode. In all experimental setups, the alignment of the crystallographic $c$ axis to the scattering plane was made when mounting the sample to the holder, with no possibility of further adjustment in vacuum. This might lead to inaccuracies when comparing measurements on different samples or along $a^*$ and $b^*$.

**Temperature dependence** In addition to the data presented in Fig. 4, we have also measured the temperature dependence of the superstructure peak, using the energy-integrated RXS on the underdoped $Nd_{1.2}Ba_{1.8}CuO_7$ thin film and $YBa_2CuO_{6.7}$ single crystal. The results are plotted in Fig. S3 and they confirm that the maximum intensity is observed at $T_c$. The systematic determination of the temperature at which where the CDW peak vanishes is complicated by the lesser sensitivity of the energy integrated measurements (weak signal on a large fluorescent background). From the data displayed in Fig. S3, the onset of charge fluctuations appears above $\geq 150$K for the underdoped samples with $T_c$ = 61 and 65 K .

**Additional information** The two-dimensionality of the CDW was verified in two ways. The comparison of REXS data measured at 130° scattering angle with the diffractometer data at 154° (Fig. 4 A,B) indicates that the CDW peak is found at exactly the same $q_{//}$ irrespective of the different value of the momentum perpendicular to the $CuO_2$ planes, (0.31,0,1.29) and (0.31,0,1.44) respectively. We have also measured, for $Nd_{1.2}Ba_{1.8}Cu_3O_7$, $T_c = 65K$, the scattering map in the $(a^*, c^*)$ plane (Fig. S1), which confirms that there is little or no dependence

of the scattering cross section along the $c^*$ direction. We can, however, not rule out short-range correlations extending over 1-2 unit cells along the $c$-axis.

The theoretical lines of Fig. 2 B are obtained from the atomic cross sections for $\pi$ and $\sigma$ incident polarization (illustrated in Fig. S4) as explained in Ref. (*26*). Those same cross sections can be multiplied by the structure factor for a 2D antiferromagnetic lattice to obtain the RIXS intensities from spin waves (*25*) of parent compounds. The atomic cross sections were calculated for a ground state with $(x^2-y^2)^{\downarrow}$ single hole symmetry and $(x^2-y^2)^{\downarrow}$ and $(x^2-y^2)^{\uparrow}$ final state for the charge and spin-flip scattering channel respectively. The spin was assumed to be oriented along the (110) direction. In case of spin fluctuations bringing the spin to point in different directions, the results would not be very different: both channels depend only on the angle $\theta_s$ between the spin and the $c$ axis but not on the in-plane spin direction. In explicit we have

$$\frac{I_{\pi}^{\mathrm{charge}}}{I_{\sigma}^{\mathrm{charge}}} = \frac{[4\sin^2(\delta-\theta)+\cos^2\theta_s]\sin^2(\delta+\theta)}{4+\cos^2\theta_s\sin^2(\delta-\theta)} \tag{S1}$$

$$\frac{I_{\pi}^{\mathrm{spin}}}{I_{\sigma}^{\mathrm{spin}}} = \frac{\sin^2(\delta+\theta)}{\sin^2(\delta-\theta)} \tag{S2}$$

where $\delta$ is the angle between the $c^*$ axis and q and $\theta$ is 1/2 of the scattering angle $2\theta$. In the $\pi/\sigma$ ratios, the structure factor cancels out (*48*) because it is the same for the two incident polarizations for each final state. In this way we do not need to make any assumptions about the scattering structure factor when trying to determine whether a given spectral feature originates from spin or charge scattering, as in Fig. 2 B. The experimental data in Fig. 2 B were corrected for self-absorption effects. The correction is very small (negligible on the scale of the plot) for $q_{//} < 0$, and sizable for $q_{//} > 0$. In the latter case $\frac{I_{\pi}^{\mathrm{charge}}}{I_{\sigma}^{\mathrm{charge}}}$ was divided by 1.3 - 1.7 and $\frac{I_{\pi}^{\mathrm{spin}}}{I_{\sigma}^{\mathrm{spin}}}$ by 0.55 - 0.75 over the 0.23 r.l.u - 0.37 r.l.u. range. This correction improves the agreement between theoretical prediction and experimental data, but the very distinct $\pi/\sigma$ intensity ratio of spin and charge channels at positive $q_{//}$ is already clearly visible in the raw data.

We end our discussion with a remark about the experimental methodology of our study. The CDW correlations presented here were first detected on an energy-resolving RXS spectrometer, where the signal-to-background ratio exceeded 1:1 (Figs. 1 D and 4 A). While this observation was subsequently reproduced on an energy-integrating RXS diffractometer, the sensitivity obtained there was an order of magnitude lower, due to the large diffuse inelastic background dominating the RXS signal (Fig. 4 B). The data measured on the former instrument benefit from a 20 times higher signal-to-background ratio, while the energy-integrated scans exhibit a higher overall intensity and hence a lower statistical which were performed on very similar samples and conditions (*24*). In addition to its well-known capability to detect spin, charge, and orbital excitations (*49*), our experiments thus establish energy-selective RXS as a highly sensitive probe of momentum-dependent static and quasi-static electronic correlations in transition metal oxides.

While this manuscript was being revised, we became aware of a study that confirmed our results for $YBa_2Cu_3O_{6.67}$. (*50*).

## Tables

| **Sample** | $a$ **(Å)** | $b$ **(Å)** | $c$ **(Å)** | $T_c$ **(K)** | $p$ |
|---|---|---|---|---|---|
| $YBa_2Cu_3O_{6.35}$ | 3.845 | 3.871 | 11.781 | 10 | 0.06 |
| $YBa_2Cu_3O_{6.45}$ | 3.839 | 3.875 | 11.761 | 35 | 0.08 |
| $Nd_{1.2}Ba_{1.8}Cu_3O_7$ (30 nm) | 3.905 | 3.905 | 11.7 | 56 | 0.09 |
| $YBa_2Cu_3O_{6.5}$ | 3.829 | 3.875 | 11.731 | 60 | 0.11 |
| $Nd_{1.2}Ba_{1.8}Cu_3O_7$ (100 nm) | 3.885 | 3.92 | 11.7 | 65 | 0.11 |
| $YBa_2Cu_3O_{6.6}$ | 3.82 | 3.87 | 11.7 | 61 | 0.12 |
| $YBa_2Cu_3O_{6.7}$ | 3.826 | 3.880 | 11.709 | 69 | 0.13 |
| $YBa_2Cu_4O_8$ | 3.84 | 3.87 | 27.25 | 80 | 0.14 |
| $YBa_2Cu_3O_7$ (100 nm) | 3.82 | 3.88 | 11.68 | 91 | 0.16 |
| $NdBa_2Cu_3O_7$ (100 nm) | 3.86 | 3.92 | 11.74 | 92 | 0.16 |
| $YBa_2Cu_3O_7$ | 3.817 | 3.884 | 11.681 | 90 | 0.17 |
| $Y_{0.85}Ca_{0.15}Ba_2Cu_3O_7$ | 3.89 | 3.88 | 11.695 | 75 | 0.21 |

Table S1: Composition, lattice parameters ($a$, $b$, $c$), transition temperature ($T_c$) and doping ($p$ holes per Cu2 atom) of the investigated systems.

## Figures

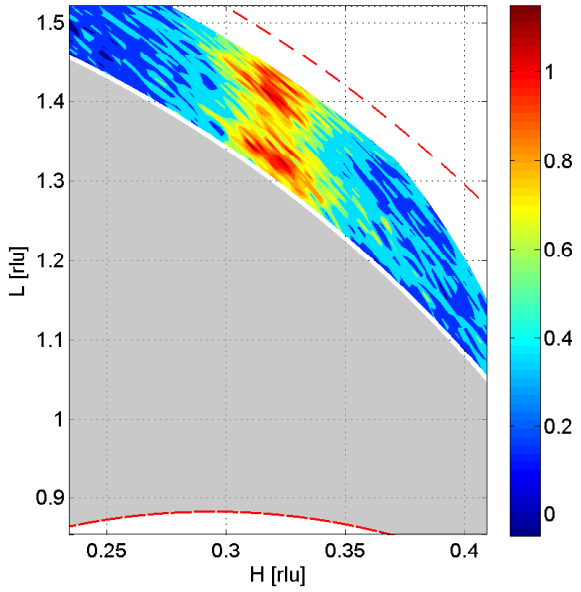


Figure S1: Color map of the scattering intensity in the $a^*c^*$ plane measured at $T$=15 K in the energy-integrated mode for $Nd_{1.2}Ba_{1.8}Cu_3O_7$, $T_c$ = 65 K. A non constant background, equal to the intensity at 200K, has been subtracted. The intensity is only weakly modulated along $c^*$ ($L$ index), and the maximum is at constant $H$ value, indicating that the CDW has intrinsic 2D nature: $H = q_{//}$ is thus the meaningful wave vector in this experiment. The red dashed and dash-dotted line indicate the limits set by the maximum value of $q$ (for $2\theta = 180°$ and the Bragg geometry limit for a (001) oriented surface respectively, for photons of 931 eV energy. Actually the meaningful data collection region is set by the signal to noise ratio, drastically decreasing when moving away from backscattering geometry: the grey area indicates a severe diffuse contamination region for this specific sample, corresponding to $2\theta_{\text{min}} \leq 130°$.

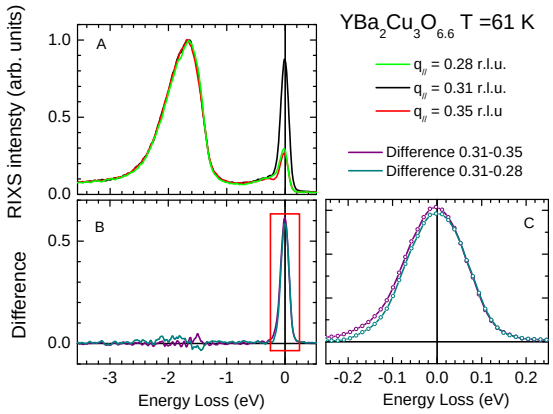


Figure S2: A) RIXS intensity at $q_{//}$=0.28, 0.31 and 0.35 r.l.u. for the $YBa_2Cu_3O_{6.6}$ sample at $T \simeq T_c$. B) Difference between the spectra measured at $q_{//} = 0.31$ and 0.28 r.l.u., and $q_{//} = 0.31$ and 0.35 r.l.u.. C) Low energy enhancement of the panel B.

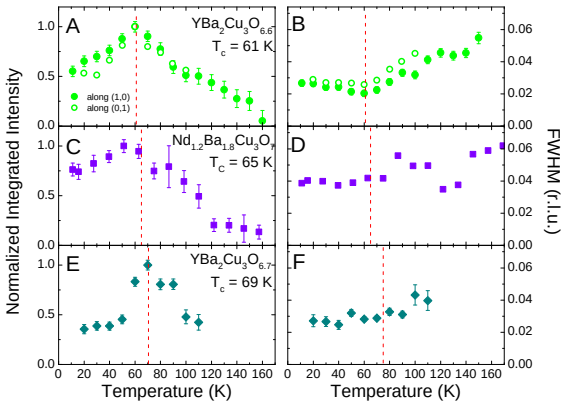


Figure S3: Temperature dependence of the CDW signal intensity and full-width-at-half-maximum (FWHM) in underdoped $YBa_2Cu_3O_{6.6}$ (A, B), $Nd_{1.2}Ba_{1.8}Cu_3O_7$ (C, D), and $YBa_2Cu_3O_{6.7}$ (E, F), measured using energy integrated RXS.

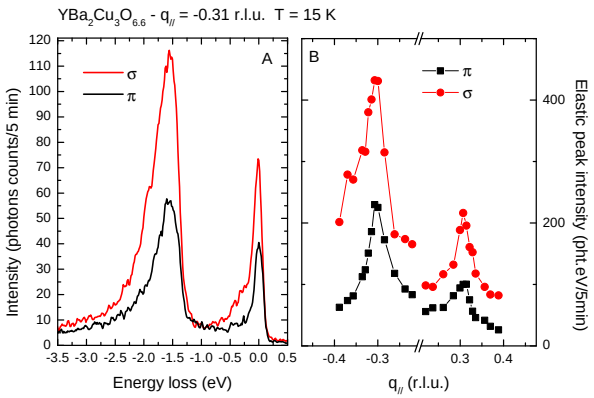


Figure S4: A) Typical RIXS spectra obtained at the Cu $L3$ edge on $YBa_2Cu_3O_{6.6}$ in $\sigma$ and $\pi$ polarization for $q_{//} = -0.31$ r.l.u. B) Momentum dependence of the integrated intensity of the quasi-elastic line. The theoretical ratio between the absolute scattering intensities in the two channels is given by equation S2 and displayed in Fig. 2 B, and is in excellent agreement with the experimental points. It must be noted that Fig. 2D has been obtained by normalizing these data to the inelastic intensity, which scales with the absorption cross section similarly to the elastic intensity, thus leading to almost identical curves for $\sigma$ and $\pi$ as shown in Fig. 2D.

**References and Notes**


1. M. Vojta, Lattice symmetry breaking in cuprate superconductors: Stripes, nematics, and superconductivity. *Adv. Phys.* **58**, 699 (2009). doi:10.1080/00018730903122242

2. R. H. He *et al*., From a single-band metal to a high-temperature superconductor via two thermal phase transitions. *Science* **331**, 1579 (2011). doi:10.1126/science.1198415 Medline

3. J. M. Tranquada, B. J. Sternlieb, J. D. Axe, Y. Nakamura, S. Uchida, Evidence for stripe correlations of spins and holes in copper-oxide superconductors. *Nature* **375**, 561 (1995). doi:10.1038/375561a0

4. P. Abbamonte *et al*., Spatially modulated "Mottness" in $La_{2-x}Ba_xCuO_4$. *Nat. Phys.* **1**, 155 (2005). doi:10.1038/nphys178

5. R. J. Birgeneau, C. Stock, J. M. Tranquada, K. Yamada, Magnetic neutron scattering in hole-doped cuprate superconductors. *J. Phys. Soc. Jpn.* **75**, 111003 (2006). doi:10.1143/JPSJ.75.111003

6. S. A. Kivelson *et al*., How to detect fluctuating stripes in the high-temperature superconductors. *Rev. Mod. Phys.* **75**, 1201 (2003). doi:10.1103/RevModPhys.75.1201

7. R. Liang, D. A. Bonn, W. N. Hardy, Evaluation of $CuO_2$ plane hole doping in $YBa_2Cu_3O_{6+x}$ single crystals. *Phys. Rev. B* **73**, 180505 (2006). doi:10.1103/PhysRevB.73.180505

8. X. F. Sun, K. Segawa, Y. Ando, Metal-to-insulator crossover in $YBa_2Cu_3O_y$ probed by low-temperature quasiparticle heat transport. *Phys. Rev. Lett.* **93**, 107001 (2004). doi:10.1103/PhysRevLett.93.107001 Medline

9. R. Daou *et al*., Broken rotational symmetry in the pseudogap phase of a high-$T_c$ superconductor. *Nature* **463**, 519 (2010). doi:10.1038/nature08716 Medline

10. F. Laliberté *et al*., Fermi-surface reconstruction by stripe order in cuprate superconductors. *Nat. Commun.* **2**, 432 (2011). doi:10.1038/ncomms1440 Medline

11. H. F. Fong *et al*., Spin susceptibility in underdoped $YBa_2Cu_3O_{6+x}$. *Phys. Rev. B* **61**, 14773 (2000). doi:10.1103/PhysRevB.61.14773

12. P. C. Dai, H. A. Mook, R. D. Hunt, F. Dogan, Evolution of the resonance and incommensurate spin fluctuations in superconducting $YBa_2Cu_3O_{6+x}$. *Phys. Rev. B* **63**, 054525 (2001). doi:10.1103/PhysRevB.63.054525

13. C. Stock *et al*., From incommensurate to dispersive spin-fluctuations: The high-energy inelastic spectrum in superconducting $YBa_2Cu_3O_{6.5}$. *Phys. Rev. B* **71**, 024522 (2005). doi:10.1103/PhysRevB.71.024522

14. V. Hinkov *et al*., Spin dynamics in the pseudogap state of a high-temperature superconductor. *Nat. Phys.* **3**, 780 (2007). doi:10.1038/nphys720

15. N. Doiron-Leyraud *et al*., Quantum oscillations and the Fermi surface in an underdoped high-Tc superconductor. *Nature* **447**, 565 (2007). doi:10.1038/nature05872 Medline

16. N. Harrison, S. E. Sebastian, Protected nodal electron pocket from multiple-Q ordering in underdoped high temperature superconductors. *Phys. Rev. Lett.* **106**, 226402 (2011). doi:10.1103/PhysRevLett.106.226402 Medline

17. T. Wu *et al*., Magnetic-field-induced charge-stripe order in the high-temperature superconductor $YBa_2Cu_3O_y$. *Nature* **477**, 191 (2011). doi:10.1038/nature10345 Medline

18. N. H. Andersen *et al*., Superstructure formation and the structural phase diagram of $YBa_2Cu_3O_{6+x}$. *Physica C* **317–318**, 259 (1999). doi:10.1016/S0921-4534(99)00066-0

19. J. Strempfer *et al*., Oxygen superstructures throughout the phase diagram of $(Y,Ca)Ba_2Cu_3O_{6+x}$. *Phys. Rev. Lett.* **93**, 157007 (2004). doi:10.1103/PhysRevLett.93.157007 Medline

20. Materials and methods are available as supplementary materials on *Science* Online.

21. G. Ghiringhelli *et al*., Low energy electronic excitations in the layered cuprates studied by copper $L_3$ resonant inelastic x-ray scattering. *Phys. Rev. Lett.* **92**, 117406 (2004). doi:10.1103/PhysRevLett.92.117406 Medline

22. L. Braicovich *et al*., Magnetic excitations and phase separation in the underdoped $La_{2-x}Sr_xCuO_4$ superconductor measured by resonant inelastic x-ray scattering. *Phys. Rev. Lett.* **104**, 077002 (2010). doi:10.1103/PhysRevLett.104.077002 Medline

23. M. Le Tacon *et al*., Intense paramagnon excitations in a large family of high-temperature superconductors. *Nat. Phys.* **7**, 725 (2011). doi:10.1038/nphys2041

24. D. G. Hawthorn *et al*., Resonant elastic soft x-ray scattering in oxygen-ordered $YBa_2Cu_3O_{6+\delta}$. *Phys. Rev. B* **84**, 075125 (2011). doi:10.1103/PhysRevB.84.075125

25. L. J. P. Ament, G. Ghiringhelli, M. M. Sala, L. Braicovich, J. van den Brink, Theoretical demonstration of how the dispersion of magnetic excitations in cuprate compounds can be determined using resonant inelastic x-ray scattering. *Phys. Rev. Lett.* **103**, 117003 (2009). doi:10.1103/PhysRevLett.103.117003 Medline

26. M. Moretti Sala *et al*., Energy and symmetry of dd excitations in undoped layered cuprates measured by Cu $L_3$ resonant inelastic x-ray scattering. *New J. Phys.* **13**, 043026 (2011). doi:10.1088/1367-2630/13/4/043026

27. D. Haug *et al*., Neutron scattering study of the magnetic phase diagram of underdoped $YBa_2Cu_3O_{6+x}$. *New J. Phys.* **12**, 105006 (2010). doi:10.1088/1367-2630/12/10/105006

28. S. B. Wilkins *et al*., Comparison of stripe modulations in $La_{1.875}Ba_{0.125}CuO_4$ and $La_{1.48}Nd_{0.4}Sr_{0.12}CuO_4$. *Phys. Rev. B* **84**, 195101 (2011). doi:10.1103/PhysRevB.84.195101

29. M. Hücker *et al*., Stripe order in superconducting $La_{2-x}Ba_xCuO_4$ ($0.095 < x < 0.155$). *Phys. Rev. B* **83**, 104506 (2011). doi:10.1103/PhysRevB.83.104506

30. W. D. Wise *et al*., Charge-density-wave origin of cuprate checkerboard visualized by scanning tunnelling microscopy. *Nat. Phys.* **4**, 696 (2008). doi:10.1038/nphys1021

31. J. E. Hoffman *et al*., A four unit cell periodic pattern of quasi-particle states surrounding vortex cores in $Bi_2Sr_2CaCu_2O_{8+\delta}$. *Science* **295**, 466 (2002). doi:10.1126/science.1066974 Medline

32. C. Howald, H. Eisaki, N. Kaneko, M. Greven, A. Kapitulnik, Periodic density-of-states modulations in superconducting $Bi_2Sr_2CaCu_2O_{8+\delta}$. *Phys. Rev. B* **67**, 014533 (2003). doi:10.1103/PhysRevB.67.014533

33. C. V. Parker *et al*., Fluctuating stripes at the onset of the pseudogap in the high-$T_c$ superconductor $Bi_2Sr_2CaCu_2O_{8+x}$. *Nature* **468**, 677 (2010). doi:10.1038/nature09597 Medline

34. O. K. Andersen *et al*., Electrons, phonons, and their interaction in $YBa_2Cu_3O_7$. *Physica C* **185-189**, 147 (1991). doi:10.1016/0921-4534(91)91964-6

35. H. Yao, D.-H. Lee, S. A. Kivelson, Fermi-surface reconstruction in a smectic phase of a high-temperature superconductor. *Phys. Rev. B* **84**, 012507 (2011). doi:10.1103/PhysRevB.84.012507

36. F. Coneri, S. Sanna, K. Zheng, J. Lord, R. De Renzi, Magnetic states of lightly hole-doped cuprates in the clean limit as seen via zero-field muon spin spectroscopy. *Phys. Rev. B* **81**, 104507 (2010). doi:10.1103/PhysRevB.81.104507

37. A. Rigamonti, F. Borsa, P. Carretta, Basic aspects and main results of NMR-NQR spectroscopies in high-temperature superconductors. *Rep. Prog. Phys.* **61**, 1367 (1998). doi:10.1088/0034-4885/61/10/002

38. B. Fauqué *et al*., Magnetic order in the pseudogap phase of high-$T_c$ superconductors. *Phys. Rev. Lett.* **96**, 197001 (2006). doi:10.1103/PhysRevLett.96.197001 Medline

39. J. Xia *et al*., Polar Kerr-effect measurements of the high-temperature $YBa_2Cu_3O_{6+x}$ superconductor: Evidence for broken symmetry near the pseudogap temperature. *Phys. Rev. Lett.* **100**, 127002 (2008). doi:10.1103/PhysRevLett.100.127002 Medline

40. V. Hinkov *et al*., Two-dimensional geometry of spin excitations in the high-transition-temperature superconductor $YBa_2Cu_3O_{6+x}$. *Nature* **430**, 650 (2004). doi:10.1038/nature02774 Medline

41. Y. T. Song, J. B. Peng, X. Wang, G. L. Sun, C. T. Lin, Ambient-condition growth of superconducting $YBa_2Cu_4O_8$ single crystals using KOH flux. *J. Cryst. Growth* **300**, 263 (2007). doi:10.1016/j.jcrysgro.2006.11.076

42. G. L. Sun, Y. T. Song, C. T. Lin, Investigation of $YBa_2Cu_4O_8$ single crystal growth by KOH flux. *Supercond. Sci. Technol.* **21**, 125001 (2008). doi:10.1088/0953-2048/21/12/125001

43. M. Salluzzo *et al*., Thickness effect on the structure and superconductivity of $Nd_{1.2}Ba_{1.8}Cu_3O_z$ epitaxial films. *Phys. Rev. B* **72**, 134521 (2005). doi:10.1103/PhysRevB.72.134521

44. V. N. Strocov *et al*., High-resolution soft x-ray beamline ADRESS at the Swiss Light Source for resonant inelastic x-ray scattering and angle-resolved photoelectron spectroscopies. *J. Synchrotron Radiat.* **17**, 631 (2010). doi:10.1107/S0909049510019862 Medline

45. G. Ghiringhelli *et al*., SAXES, a high resolution spectrometer for resonant x-ray emission in the 400–1600 eV energy range. *Rev. Sci. Instrum.* **77**, 113108 (2006). doi:10.1063/1.2372731

46. C. Dallera *et al*., Soft x-ray emission spectroscopy at ESRF beamline 26 based on a helical undulator. *J. Synchrotron Radiat.* **3**, 231 (1996). doi:10.1107/S0909049596006061 Medline

47. M. E. Dinardo *et al*., Gaining efficiency and resolution in soft x-ray emission spectrometers thanks to directly illuminated CCD detectors. *Nucl. Instrum. Methods Phys. Res. Sect. A* **570**, 176 (2007). doi:10.1016/j.nima.2006.10.024

48. L. Braicovich *et al*., Momentum and polarization dependence of single-magnon spectral weight for Cu $L_3$-edge resonant inelastic x-ray scattering from layered cuprates. *Phys. Rev. B* **81**, 174533 (2010). doi:10.1103/PhysRevB.81.174533

49. L. J. P. Ament, M. van Veenendaal, T. P. Devereaux, J. P. Hill, J. van den Brink, Resonant inelastic x-ray scattering studies of elementary excitations. *Rev. Mod. Phys.* **83**, 705 (2011). doi:10.1103/RevModPhys.83.705

50. J. Chang *et al*., preprint at http://arxiv.org/abs/1206.4333